

Article

Analytical Solution of Time-Optimal Trajectory for Heaving Dynamics of Hybrid Underwater Gliders

Mai The Vu ¹, Seong Han Kim ^{1,*}, Van P. Nguyen ², Nguyen Xuan-Mung ³, Jiafeng Huang ^{4,5}, Dong-Wook Jung ^{4,5} and Hyeung-Sik Choi ^{4,*}

¹ Department of Intelligent Mechatronics Engineering, Sejong University, Seoul 05006, Republic of Korea; maithevu90@sejong.ac.kr

² Faculty of Engineering, Dong Nai Technology University, Bien Hoa City 76000, Vietnam; nguyenvanpho@dtu.edu.vn

³ Faculty of Mechanical and Aerospace Engineering, Sejong University, Seoul 05006, Republic of Korea; xuanmung@sejong.ac.kr

⁴ Department of Mechanical Engineering, Korea Maritime & Ocean University, Busan 49112, Republic of Korea; hjf1203@g.kmou.ac.kr (J.H.); jdww0425@kmou.ac.kr (D.-W.J.)

⁵ Interdisciplinary Major of Ocean Renewable Energy Engineering, Korea Maritime and Ocean University, Busan 49112, Republic of Korea

* Correspondence: shkim8@sejong.ac.kr (S.H.K.); hchoi@kmou.ac.kr (H.-S.C.)

Abstract: Underwater vehicles have capacity limits for control inputs, within which their time-optimal trajectories (TOTs) can be formulated. In this study, the fastest trajectory for the depth control of a hybrid underwater glider (HUG) was found using buoyancy engines and propellers individually, and the decoupled heave dynamics of the HUG were defined using quadratic hydrodynamic damping. Because buoyancy engines always run at slow speeds, the buoyancy force was formulated based on the constant force rate of the engine. It was assumed that the nominal value of the heave dynamics parameters could be estimated; therefore, the analytical solution of heave dynamics could be formulated using the thrusting saturation and constant buoyancy force rate. Then, the shortest trajectory for depth control of the HUG could be established while considering the actuator saturation. To verify the effectiveness of the TOT in HUG heave dynamics, extensive tracking control simulations following the TOT were conducted. It was found that the proposed TOT helps the HUG reach the desired depth in the shortest arrival time, and its robust depth control showed good tracking performance in the presence of external bounded disturbances.

Keywords: time-optimal trajectory; heave dynamics; buoyancy engines; propellers; hybrid underwater glider



Citation: Vu, M.T.; Kim, S.H.; Nguyen, V.P.; Xuan-Mung, N.; Huang, J.; Jung, D.-W.; Choi, H.-S. Analytical Solution of Time-Optimal Trajectory for Heaving Dynamics of Hybrid Underwater Gliders. *J. Mar. Sci. Eng.* **2023**, *11*, 2216. <https://doi.org/10.3390/jmse11122216>

Academic Editor: Spyros Hirdaris

Received: 17 October 2023

Revised: 14 November 2023

Accepted: 20 November 2023

Published: 22 November 2023



Copyright: © 2023 by the authors. Licensee MDPI, Basel, Switzerland. This article is an open access article distributed under the terms and conditions of the Creative Commons Attribution (CC BY) license (<https://creativecommons.org/licenses/by/4.0/>).

1. Introduction

With the advancement of oceanography research and marine resource exploration, underwater mobile platforms have gained prominence, assuming a pivotal role in various underwater missions including resource exploration, ocean observation, environmental monitoring, and sea area investigations [1–3]. These platforms come in various types, such as remotely operated vehicles (ROVs) [4–6], autonomous underwater vehicles (AUVs) [7–9], and underwater gliders (UGs) [10–12]. Among these, the underwater glider (UG) stands out as a buoyancy-driven autonomous robot capable of converting vertical motion into horizontal movement using airfoil technology, allowing it to move forward with minimal power consumption over extended periods [13]. Utilizing fixed wings, internal masses, a ballast pump, and a rudder, this glider controls its attitude and depth by adjusting buoyancy levels, gliding effortlessly through the water column. Due to its exceptional performance, traditional cylindrical UGs have garnered significant research attention [14,15].

UGs like the Slocum [16,17], Spray [18], Seaglider [19,20], and Deepglider [21,22] were originally developed for oceanographic applications. While these buoyancy-driven gliders

have demonstrated impressive endurance and energy efficiency, they suffer from limitations in speed and maneuverability due to their restricted propulsion capabilities and external control surfaces. Hence, enhancing the efficiency of gliders necessitates a reconfiguration of their design [23–25]. One innovative approach to address these limitations involves the hybrid-driven UG equipped with a propeller, independently adjustable wings, and a controllable rudder. This innovative design incorporates a dual-mode propulsion system, augmenting the glider's speed significantly. Moreover, the integration of controllable wings and a rudder enhances the glider's maneuverability, thereby enhancing its overall versatility.

Trajectories play a pivotal role in governing the motion of autonomous systems, and their meticulous design is necessary for attaining high performance. Each underwater vehicle has a capacity limit for control inputs, including the maximum thrust of the propeller or the maximum net buoyancy force of the buoyancy engine. Time-optimal trajectories (TOTs) for these vehicles can be formulated within these constraints. Previous studies have focused on the TOT problem, such as the singular extremals of underwater vehicle systems in [26] and the design of time-efficient trajectories with constant thrust arcs in [27]. However, the latter algorithm required significant computational time for practical implementation. Rhoads et al. [28] presented a numerical method for minimum time heading control of an UG in known and time-varying flow fields. Meanwhile, Vu et al. [29] developed an energy-efficient trajectory for depth motion control in underwater vehicle systems. Their approach addressed uncertainties in bounded parameters and disturbances, utilizing a global optimal sliding mode controller with limited control input. Duc et al. [30] derived an analytical solution for the second-order nonlinear differential equation governing the heading motion of underwater vehicles. However, this research exclusively formulated the analytical solution for heading motion using propeller thrust saturation.

Achieving precise trajectory tracking amidst disturbances and uncertainties poses a significant challenge, particularly for nonlinear systems and notably in robotic systems [31–33]. Numerous control strategies have been proposed to address this issue, including sliding mode control [34,35], adaptive control [36,37], neural network control [38], backstepping control [39,40], dynamic surface control [41,42], etc. Among these approaches, sliding mode control (SMC) offers an effective approach to attain robust control for underactuated underwater vehicles. Its inherent discontinuity, characterized by switching characteristics, renders SMC a fitting choice for governing underactuated systems. Furthermore, SMCs exhibit well in handling-system parameter uncertainties and disturbances [43,44]; thus, SMC demonstrates remarkable robustness when applied to systems with uncertainties. The depth controller is imperative for an underwater vehicle to execute its mission successfully under the influence of environmental loads. Consequently, validating the performance of the designed controller through simulations becomes an indispensable step before any real-world trials. The HUG's ability to track the desired depth is hindered by two major barriers, namely steady-state error and non-zero pitch angle. Inaccurate trim and ballasting conditions were found to be the cause of this issue in a previous study by Claus et al. [45], where the depth control of a HUG using a buoyancy engine and internal moving mass was described. However, this method resulted in considerable overshoot and steady-state error in depth-keeping control, with suboptimal settling time. To overcome these issues, this study aims to design an efficient trajectory for depth control of a HUG using a buoyancy engine and thruster, with the objective of eliminating overshoot and steady-state error while maintaining the desired depth.

In this study, the goal is to design a TOT for depth control in the HUG system using buoyancy-driven propulsion and a thruster individually. A closed-form solution is presented for the pure heave dynamics under each constraint of buoyancy and thrusting force. The control input is designed based on the limits of buoyancy force, buoyancy force rate, and thruster force, and the TOT for depth control is defined to satisfy the constraints of heave dynamics and actuator saturation. To track the TOT under the presence of external

bounded disturbance, an SMC algorithm is designed, and its performance along with the proposed TOT will be verified through computer simulations.

The rest of this paper is organized as follows. The concept of TOTs for depth control of a HUG is presented in Section 2, followed by the closed-form solution of pure heave dynamics in Section 3, where maximum buoyancy force, maximum rate of buoyancy force, and minimum propeller force are considered. Section 4 defines the time-optimal trajectory, and Section 5 presents the design of robust tracking control using SMC. The robust tracking control with the proposed TOT will be simulated in Section 6 while considering the bounded disturbance. Finally, the conclusion presents the effectiveness of the proposed TOT and highlights the merits of the closed-form solution.

2. Heave Dynamics of Hybrid Underwater Glider and TOT Definition

2.1. Assumptions

In this paper, the motion of the HUG is simplified to focus solely on its heave motion. Some simplifications have been applied to enable feasible simulations of the HUG. These simplifications are outlined as follows:

- The HUG is assumed to have neutral buoyancy, with its body-fixed coordinate system centered at its mass center;
- The HUG is deeply submerged in a homogeneous, unbounded fluid, far removed from the free surface and devoid of surface effects;
- The HUG exhibits three planes of symmetry;
- To simplify the problem, only the depth motion of the HUG is considered in this paper;
- The hydrodynamic coefficients of the HUG remain constant and do not vary.

2.2. Heave Motion of HUG and TOT Definition

In this section, we propose a TOT for the heave control of HUGs, which is a challenging task due to the slow speed of the buoyancy engine. The TOT is based on the limitations of the buoyancy engine speed and saturation, as well as the thruster saturation. The six degrees-of-freedom (DOF) nonlinear equations of motion for an underwater vehicle are detailed in Fossen [46,47]. However, this paper specifically concentrates on depth control. Thus, we present the nonlinear second-order differential equation that characterizes the pure depth-plane motion of the HUG as follows:

$$\begin{aligned} (m - Z_{\dot{w}})\ddot{w} - Z_{w|w|}w|w| &= (W - B) + Z_{prop} \\ \dot{z} &= w \end{aligned} \tag{1}$$

where m , $Z_{\dot{w}}$, w , $Z_{w|w|}$, W , B , and Z_{prop} are the mass of the HUG, added mass coefficient, instantaneous velocity, cross-flow drag coefficient, weight of the HUG, buoyancy force, and thrust force, respectively.

The heave dynamics of HUGs, described by two first-order differential systems, can be represented by Equation (2), where $a = m - Z_{\dot{w}}$, $b = -Z_{w|w|}$, and f represent the control force acting on the vehicle, d is the external disturbance, $Z_{\dot{w}}$ is the added mass, and $Z_{w|w|}$ is the damping coefficient.

$$\begin{aligned} a\dot{w} + b|w|w &= f + d \\ \dot{z} &= w \end{aligned} \tag{2}$$

This paper employs an analytical approach, distinct from numerical methods, to derive TOTs. These TOTs are represented as explicit functions within unchanged closed-form expressions, enhancing the controller’s autonomous capabilities. The proposed trajectory-tracking controller ensures optimal time performance when its references (inputs) align with the TOTs, even in the presence of uncertainties. The concept of a TOT is grounded in formulating the solution of the given dynamics as a time-dependent function for a specific control input. In this context, maintaining the control input at both maximum and

minimum values during acceleration and deceleration times yields the closed-form time function representing the fastest or TOT for the given dynamics.

Table 1 provides a definition of the terms used in the proposed TOT.

Table 1. Some variables used in the TOT.

Variables	Description
f_{max}	The maximum force applied to HUG
f_{min}	The minimum force applied to HUG
z_0	Initial depth of HUG
z_5	Desired depth of HUG
w_{d1}	The velocity profile of HUG in the 1st segment
w_{d2}	The velocity profile of HUG in the 2nd segment
w_{d3}	The velocity profile of HUG in the 3rd segment
w_{d4}	The velocity profile of HUG in the 4th segment
w_{d5}	The velocity profile of HUG in the 5th segment
z_{d1}	The position profile of HUG in the 1st segment
z_{d2}	The position profile of HUG in the 2nd segment
z_{d3}	The position profile of HUG in the 3rd segment
z_{d4}	The position profile of HUG in the 4th segment
z_{d5}	The position profile of HUG in the 5th segment
\dot{w}_{d1}	The acceleration profile of HUG in the 1st segment
\dot{w}_{d2}	The acceleration profile of HUG in the 2nd segment
\dot{w}_{d3}	The acceleration profile of HUG in the 3rd segment
\dot{w}_{d4}	The acceleration profile of HUG in the 4th segment
\dot{w}_{d5}	The acceleration profile of HUG in the 5th segment

The HUG system utilizes two types of control forces: the net buoyancy force u_b produced by the buoyancy engine and the thruster force u_t generated by the thruster depicted in Figure 1. The buoyancy engine is employed for descent, requiring low energy consumption, while the thruster force is used sparingly when the vehicle approaches the desired depth and to maintain the HUG at that depth. By switching between these two forces, the HUG can be precisely controlled to reach the desired depth. To minimize the use of thruster force, it should only be applied once the vehicle attains neutral buoyancy.

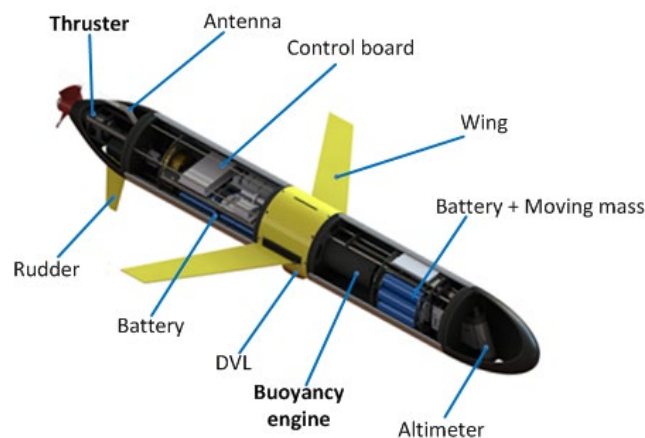


Figure 1. Buoyancy engine and thruster location in the HUG system.

The control strategy for the heaving motion of the HUG system is depicted in Figure 2a, which shows the buoyancy force of the buoyancy engine as a dashed blue line. The up slope and down slope represent the compression and expansion rates of air in the cylinder, respectively. The designed thruster force is represented by the solid orange line.

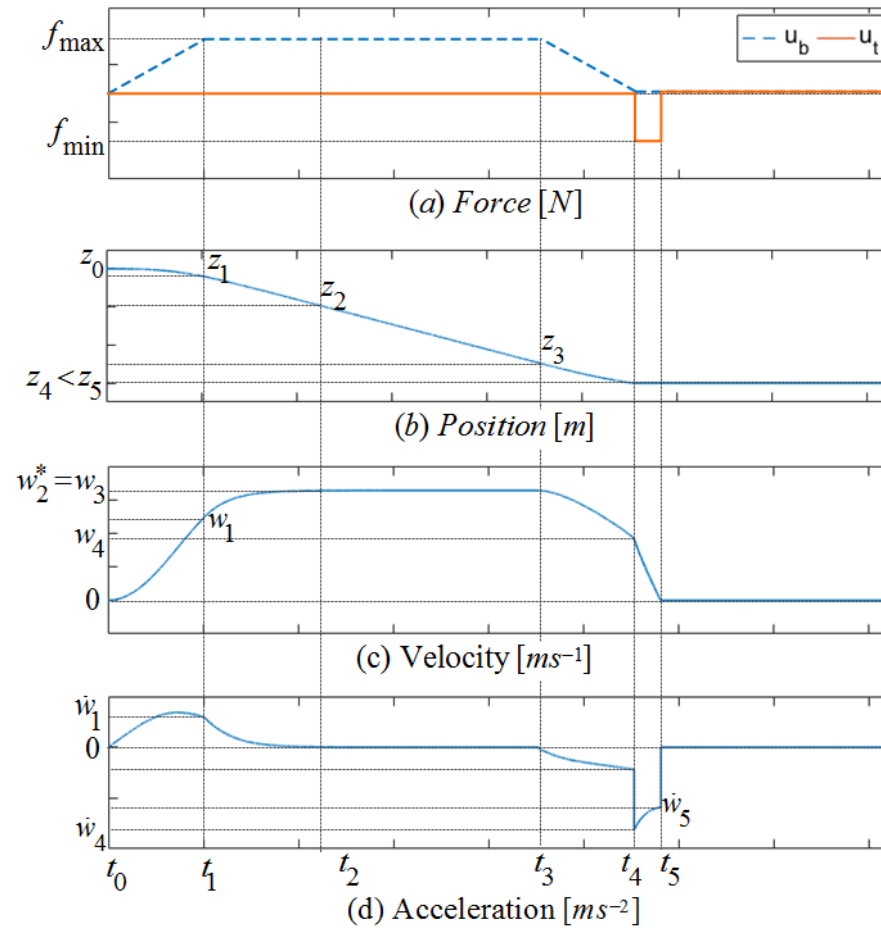


Figure 2. The profile of the proposed TOT: (a) force, (b) position, (c) velocity, and (d) acceleration.

In order to control the depth of the HUG system, the constant rate of the buoyancy force needs to be considered. This constant rate of the buoyancy force can be expressed as c_{max} and c_{min} for the maximum and minimum speeds, respectively. Thus, the buoyancy force can be formulated as $c_{max}(t - t_0)$ and $c_{min}(t - \alpha)$, where t_0 and α are the initial times for the descending motion and neutral condition, respectively. To ensure precise depth control, it is necessary to define five different time periods, as described in Figure 2. The first segment is from t_0 to t_1 , and the dynamics of this period can be deduced from Equation (3). It is important to note that $t_1 = t_0 + \frac{f_{max}}{c_{max}}$ plays a key role in this period. The dynamics equations for the second and third segments, which are from t_1 to t_2 and from t_2 to t_3 , respectively, can be defined as Equation (4). Similarly, the dynamics of the fourth and fifth segments can be established as Equations (5) and (6), respectively. By solving all these dynamics, the TOT for the pure depth plant of the HUG system can be defined. However, it should be noted that this concept is only applicable during deep operation, as the HUG should reach maximum heaving velocity as depicted in Figure 2d, which can be expressed by the condition $z_5 \geq (z_2 - z_0) + (z_4 - z_3)$. This concept is effective in achieving precise depth control at depths of several hundred meters.

$$a\ddot{w}_d + b\dot{w}_d^2 = c_{max}(t - t_0) \tag{3}$$

$$a\dot{w}_d + bw_d^2 = f_{max} \tag{4}$$

$$a\dot{w}_d + bw_d^2 = c_{min}(t - \alpha) \tag{5}$$

$$a\dot{w}_d + bw_d^2 = f_{min} \tag{6}$$

3. Analytical Solution of TOT in Heave Dynamics of HUG Using Buoyancy and Thruster Force Individually

3.1. TOT in the 1st Segment with Positive Force Rate from Buoyancy Engine

The heave dynamics in this segment can be described by Equation (7), which can be rewritten as Equation (8) by defining the variable w_{d1} as $\frac{a}{b} \frac{\dot{y}}{y}$. The solution to Equation (8) involves the use of the Airy function, which can be solved using an alternative function y , as presented in Equation (9).

$$a\dot{w}_{d1} + bw_{d1}^2 = c_{max}(t - t_0) \tag{7}$$

$$\frac{a^2}{b} \left(\frac{\ddot{y}}{y} - \frac{\dot{y}^2}{y^2} \right) + \frac{a^2 \dot{y}^2}{by^2} = c_{max}(t - t_0) \tag{8}$$

$$\Leftrightarrow \frac{a^2}{b} \frac{\ddot{y}}{y} = c_{max}(t - t_0) \tag{9}$$

$$y(t) = a_0 y_0(t) + a_1 y_1(t) \tag{9}$$

To define the components of function $y(t)$, we can use the following equations:

$$y_0(t) = 1 + \frac{\sigma_1(t - t_0)^3}{6} + \frac{\sigma_1^2(t - t_0)^6}{180} + \frac{\sigma_1^3(t - t_0)^9}{12960} \tag{10}$$

$$y_1(t) = (t - t_0) + \frac{\sigma_1(t - t_0)^4}{12} + \frac{\sigma_1^2(t - t_0)^7}{504} + \frac{\sigma_1^3(t - t_0)^{10}}{45360} \tag{11}$$

$$\sigma_1 = \frac{bc_{max}}{a^2} \tag{12}$$

Having the function $y(t)$ defined, its first and second derivatives can be calculated as follows:

$$\dot{y}(t) = a_0 \dot{y}_0(t) + a_1 \dot{y}_1(t) \tag{13}$$

$$\ddot{y}(t) = a_0 \ddot{y}_0(t) + a_1 \ddot{y}_1(t) \tag{14}$$

Subsequently, the velocity trajectory can be represented as Equation (15) using the alternative function y , while the acceleration trajectory can be obtained by taking the derivative of the velocity trajectory, as presented in Equation (16). Finally, the position trajectory can be derived by integrating the velocity trajectory and is given by Equation (17), with C_0 defined as Equation (18).

$$w_{d1} = \frac{a}{b} \frac{\dot{y}}{y} \tag{15}$$

$$\dot{w}_{d1} = \frac{a}{b} \left(\frac{\ddot{y}}{y} - \frac{\dot{y}^2}{y^2} \right) \tag{16}$$

$$z_{d1} = \frac{a}{b} \ln|y| + C_0 \tag{17}$$

$$C_0 = z_0 - \frac{a}{b} \ln|a_0 p_1 + a_1 p_2| \tag{18}$$

where $p_1 = y_0(t_0)$, $p_2 = y_1(t_0)$, $p_3 = \dot{y}_0(t_0)$, $p_4 = \dot{y}_1(t_0)$, $a_0 = 1$, and $a_1 = -\frac{p_3}{p_4}a_0$.

3.2. TOT in the 2nd Segment with Maximum Force from Buoyancy Engine

The second segment's dynamics are calculated using the maximum input, as shown in Equation (19). In [29], a closed-form solution was derived for these dynamics, which can be expressed as Equations (20)–(22) in this work.

$$a\dot{w}_{d2} + bw_{d2}^2 = f_{max} \tag{19}$$

$$w_{d2} = \frac{2\sqrt{f_{max}/b}}{1 + e^{\frac{2}{a}\sqrt{bf_{max}}(t+C_1)}} - \sqrt{\frac{f_{max}}{b}} \tag{20}$$

$$\dot{w}_{d2} = \frac{4f_{max}}{a} \frac{e^{-\frac{2}{a}\sqrt{bf_{max}}(t+C_1)}}{\left(1 + e^{-\frac{2}{a}\sqrt{bf_{max}}(t+C_1)}\right)^2} \tag{21}$$

$$z_{d2} = \frac{a}{b} \ln\left(1 + e^{\frac{2}{a}\sqrt{bf_{max}}(t+C_1)}\right) - \sqrt{\frac{f_{max}}{b}}t + C_2 \tag{22}$$

The values of the constants C_1 and C_2 in this work are obtained through a different approach than that used in [29] due to the variation in input geometries. These constants can be calculated at time t_1 , and their formulas are given in Equations (23) and (24), respectively.

$$C_1 = \frac{-a}{2\sqrt{bf_{max}}} \ln\left(\frac{2\sqrt{f_{max}/b}}{w_1 + \sqrt{f_{max}/b}} - 1\right) - t_1 \tag{23}$$

$$C_2 = z_1 - \frac{a}{b} \ln\left(1 + e^{\frac{2}{a}\sqrt{bf_{max}}(t_1+C_1)}\right) + \sqrt{\frac{f_{max}}{b}}t_1 \tag{24}$$

3.3. TOT in the 3rd Segment with Constant Velocity

The typical desired depth for an underwater glider is usually several hundred meters, which means that the constant velocity in the heave motion will be attained for deep-sea HUGs. As a result, the dynamics of the third segment are always present, as defined in Equation (25), and the constant velocity in this segment equals w_2^* or $w_3 = w_2^*$. By using Equation (26), the position trajectory can be determined, and the boundary constant C_3 can be obtained as Equation (27).

$$a\dot{w}_{d3} + bw_{d3}^2 = f_{max} \tag{25}$$

$$z_{d3} = w_3t + C_3 \tag{26}$$

$$C_3 = z_2 - w_2t_2 \tag{27}$$

3.4. TOT in the 4th Segment with Negative Force Rate from Buoyancy Engine

In this segment, the net buoyancy force begins to decrease to zero, and its delay is defined in Equation (29). To compute the trajectory, we will use the alternative function $k(t)$.

$$a\dot{w}_{d4} + bw_{d4}^2 = c_{min}(t - \alpha) \tag{28}$$

$$\alpha = t_3 - \frac{f_{max}}{c_{min}} \tag{29}$$

The velocity trajectory of this segment can be solved using Equation (30), and its derivative gives the acceleration trajectory, as shown in Equation (31). Finally, the posi-

tion trajectory can be found using Equation (32) with the boundary condition given in Equation (33).

$$w_{d4} = \frac{a \dot{k}}{b k} \tag{30}$$

$$\dot{w}_{d4} = \frac{a}{b} \left(\frac{\ddot{k}}{k} - \frac{\dot{k}^2}{k^2} \right) \tag{31}$$

$$z_{d4} = \frac{a}{b} \ln|k| + C_4 \tag{32}$$

$$C_4 = z_0 - \frac{a}{b} \ln|a_0 p_1 + a_1 p_2| \tag{33}$$

where

$$\begin{aligned} k(t) &= n_0 k_0(t) + n_1 k_1(t); y_0(t) = 1 + \frac{\sigma_4(t-\alpha)^3}{6} + \frac{\sigma_4^2(t-\alpha)^6}{180} + \frac{\sigma_4^3(t-\alpha)^9}{12960}; \\ y_1(t) &= (t-\alpha) + \frac{\sigma_1(t-\alpha)^4}{12} + \frac{\sigma_1^2(t-\alpha)^7}{504} + \frac{\sigma_1^3(t-\alpha)^{10}}{45360}; \sigma_4 = \frac{bc_{min}}{a^2}; \\ \dot{k}(t) &= n_0 \dot{k}_0(t) + n_1 \dot{k}_1(t); \ddot{k}(t) = a_0 \ddot{k}_0(t) + a_1 \ddot{k}_1(t). \end{aligned}$$

3.5. TOT in the 5th Segment with Minimum Input from the Thruster

The thruster is employed at the end of the TOT in the HUG system since it has a quicker response compared to the buoyancy force. Although the thruster consumes more power, it is still a feasible option for the HUG system as it is utilized for only a brief duration in the TOT. Unlike the buoyancy force that requires a relatively longer time to change its effect, the thruster can quickly adjust the glider’s position, making it the preferred choice for maintaining the desired depth during the final segment of the TOT.

$$a \dot{w}_{d5} + b w_{d5}^2 = f_{min} \tag{34}$$

The fifth segment is crucial for the HUG system to reach the desired depth as quickly as possible, and the thruster force is used for this purpose. The dynamics of this segment can be expressed as Equation (34), which is a solution presented in a previous work [29]. By rewriting the solution, the velocity, acceleration, and position trajectories can be obtained as Equations (35)–(37), respectively.

$$w_{d5} = \sqrt{\frac{-f_{min}}{b}} \tan \left(-\frac{\sqrt{-b f_{min}}}{a} (t + C_5) \right) \tag{35}$$

$$\dot{w}_{d5} = \frac{f_{min}}{a} \frac{1}{\cos^2 \left(-\frac{\sqrt{-b f_{min}}}{a} (t + C_5) \right)} \tag{36}$$

$$z_{d5} = \frac{a}{b} \ln \left| \cos \left(-\frac{\sqrt{-b f_{min}}}{a} (t + C_5) \right) \right| + C_6 \tag{37}$$

At the time instant t_4 , the values of the constants C_5 and C_6 are calculated using the expressions given in Equations (38) and (39), respectively.

$$C_5 = \frac{-a}{\sqrt{-b f_{min}}} \arctan \left(\frac{w_4}{\sqrt{\frac{-f_{min}}{b}}} \right) - t_4 \tag{38}$$

$$C_6 = z_4 - \frac{a}{b} \ln \left| \cos \left(-\frac{\sqrt{-bf_{min}}}{a} (t_4 + C_5) \right) \right| \tag{39}$$

4. Closed-Form Solution for TOT in Heave Dynamics of HUG

The assumptions made for the forces and rates in the HUG system are critical for its operation. Specifically, it is assumed that the maximum force generated by the buoyancy engine is f_{max} , while the thruster’s minimum force is f_{min} . Additionally, the maximum and minimum rates of the net buoyancy force generated by the buoyancy engine are c_{max} and c_{min} , respectively.

A solution for the TOT can be obtained by solving the heave dynamics at specific time instances, namely t_1, t_2, t_3, t_4 , and t_5 , for the individual dynamics of buoyancy engines and thrusters. Here, $t_1 = t_0 + \frac{f_{max}}{c_{max}}$ and $t_4 - t_3 = \frac{f_{min}}{c_{min}}$ due to the delay in the buoyancy force. The problem is defined with the given information such as the initial conditions $t_0 = 0, w_0 = 0, \dot{w}_0 = 0$, and z_0 and the final conditions w_5, \dot{w}_5 , and z_5 .

4.1. Find z_1, w_1 and \dot{w}_1

First, we define some parameters as $p_1 = y_0(t_0); p_2 = y_1(t_0); p_3 = \dot{y}_0(t_0); p_4 = \dot{y}_1(t_0); p_5 = \ddot{y}_0(t_0); p_6 = \ddot{y}_1(t_0); q_1 = y_0(t_1); q_2 = y_1(t_1); q_3 = \dot{y}_0(t_1); q_4 = \dot{y}_1(t_1); q_5 = \ddot{y}_0(t_1); q_6 = \ddot{y}_1(t_1); l_1 = k_0(t_3 - t_4); l_2 = k_1(t_3 - t_4); l_3 = \dot{k}_0(t_3 - t_4); l_4 = \dot{k}_1(t_3 - t_4); l_5 = \ddot{k}_0(t_3 - t_4); l_6 = \ddot{k}_1(t_3 - t_4); h_1 = k_0(0); h_2 = k_1(0); h_3 = \dot{k}_0(0); h_4 = \dot{k}_1(0); h_5 = \ddot{k}_0(0); h_6 = \ddot{k}_1(0); t_3 - t_4 = \frac{f_{max}}{c_{min}}$.

$$\begin{aligned} & \begin{cases} w_{d1}(t_0) = w_0 \\ \dot{w}_{d1}(t_0) = \dot{w}_0 \\ z_{d1}(t_0) = z_0 \end{cases} \\ \Leftrightarrow & \begin{cases} \dot{y}_0(t_0) = 0 \\ \ddot{y}_0(t_0) = 0 \\ \frac{a}{b} \ln |y(t_0)| + C_0 = z_0 \end{cases} \\ \Leftrightarrow & \begin{cases} a_0 p_3 + a_1 p_4 = 0 \\ a_0 p_5 + a_1 p_6 = 0 \\ C_0 = z_0 - \frac{a}{b} \ln |a_0 p_1 + a_1 p_2| \\ a_1 = -\frac{p_3}{p_4} a_0 \end{cases} \\ \Leftrightarrow & \begin{cases} a_0 p_5 + a_1 p_6 = 0 \\ C_0 = z_0 - \frac{a}{b} \ln |a_0 p_1 + a_1 p_2| \end{cases} \end{aligned} \tag{40}$$

Based on the above equations, constraints on the initial conditions of w_0, \dot{w}_0 , and z_0 can be defined as Equation (40). Solving these constraints yields the constant C_0 and enables the relationship between a_0 and a_1 to be established.

Assuming the parameter $a_0 = 0$, the set of constraints defined in Equation (40) can be solved as follows.

$$a_1 = -\frac{p_3}{p_4} a_0 \tag{41}$$

$$C_0 = z_0 - \frac{a}{b} \ln |a_0 p_1 + a_1 p_2| \tag{42}$$

$$z_1 = \frac{a}{b} \ln |a_0 q_1 + a_1 q_2| + C_0 \tag{43}$$

$$w_1 = \frac{a}{b} \left(\frac{a_0 q_3 + a_1 q_4}{a_0 q_1 + a_1 q_2} \right) \tag{44}$$

$$\dot{w}_1 = \frac{a}{b} \left(\frac{a_0 q_5 + a_1 q_6}{a_0 q_1 + a_1 q_2} - \frac{(a_0 q_3 + a_1 q_4)^2}{(a_0 q_1 + a_1 q_2)^2} \right) \tag{45}$$

The calculation of the remaining unknowns can be computed in subsequent steps once the first boundary is solved.

4.2. Find t_2 , z_2 , w_2 , and \dot{w}_2

Based on the given time t_1 and the previously obtained value of w_1 , the boundary constants C_1 and C_2 can be determined using the following equations.

$$C_1 = \frac{-a}{2\sqrt{bf_{max}}} \ln \left(\frac{2\sqrt{f_{max}/b}}{w_1 + \sqrt{f_{max}/b}} - 1 \right) - t_1 \tag{46}$$

$$C_2 = z_1 - \frac{a}{b} \ln \left(1 + e^{\frac{2}{a}\sqrt{bf_{max}}(t_1+C_1)} \right) + \sqrt{\frac{f_{max}}{b}} t_1 \tag{47}$$

The logarithmic function requires a non-zero argument; therefore, we define w_{2c} as Equation (48), which is then used to calculate t_2 in Equation (49) instead of using w_2 . It is worth noting that a slight error in this conversion is considered acceptable.

$$w_{2c} = \varepsilon \sqrt{\frac{f_{max}}{b}} (\varepsilon \approx 1) \tag{48}$$

$$t_2 = t_{2c} = \frac{-a}{2\sqrt{bf_{max}}} \ln \left(\frac{2\sqrt{f_{max}/b}}{w_{2c} + \sqrt{f_{max}/b}} - 1 \right) - C_1 \tag{49}$$

After calculating the time t_2 using the expression in Equation (49), the trajectories at this time can be obtained as Equations (50)–(52).

$$z_2 = \frac{a}{b} \ln \left(1 + e^{\frac{2}{a}\sqrt{bf_{max}}(t_{2c}+C_1)} \right) - \sqrt{\frac{f_{max}}{b}} t_{2c} + C_2 \tag{50}$$

$$w_2 = \frac{2\sqrt{f_{max}/b}}{1 + e^{\frac{2}{a}\sqrt{bf_{max}}(t_{2c}+C_1)}} - \sqrt{\frac{f_{max}}{b}} \tag{51}$$

$$\dot{w}_2 = \frac{4f_{max}}{a} \frac{e^{-\frac{2}{a}\sqrt{bf_{max}}(t_{2c}+C_1)}}{\left(1 + e^{-\frac{2}{a}\sqrt{bf_{max}}(t_{2c}+C_1)} \right)^2} \tag{52}$$

4.3. Find w_3 , z_4 and w_4

The order of solving the TOTs cannot follow a sequential approach from the first to the fifth segment. As such, it is necessary to define trajectories for the fourth segment before the third and fifth segments. Constant C_3 can be calculated using information from the second segment and is given by Equation (53). The constant velocity in the third segment can then be obtained using Equation (54).

$$C_3 = z_2 - w_2 t_2 \tag{53}$$

$$w_3 = \sqrt{\frac{f_{max}}{b}} \tag{54}$$

The velocity at time t_4 can be obtained using Equation (55).

$$w_4 = \frac{-\frac{a}{b}l_3 + l_1w_3}{l_4 - \frac{b}{a}l_2w_3} \tag{55}$$

To estimate the position trajectory at time t_4 , we approximate $\chi \approx 0$, $\chi > 0$. This allows us to estimate the arbitrary constants n_0 and n_1 of the Airy solution in the function $k(t)$, which can be obtained using Equations (57) and (58).

$$\beta = \frac{b}{a}w_4 \tag{56}$$

$$n_0 = \frac{\sqrt{\chi}}{\sqrt{l_1l_5 + \beta l_2l_5 + \beta l_1l_6 + \beta^2 l_2l_6 - l_3^2 - \beta^2 l_4^2 - 2\beta l_3l_4}} \tag{57}$$

$(\chi \approx 0, \chi > 0)$

$$n_1 = \beta n_0 \tag{58}$$

The computation of the distance from t_3 to t_4 is then obtained by Equation (59) in the following.

$$\Delta z_{43} = \frac{a}{b} \ln \left| \frac{n_0 h_1 + n_1 h_2}{n_0 l_1 + n_1 l_2} \right| \tag{59}$$

The distance travelled from t_4 to t_5 can be determined by using Equation (60).

$$\Delta z_{54} = \frac{a}{b} \ln \sqrt{1 - \frac{w_4^2}{f_{min}/b}} \tag{60}$$

Finally, based on the distance Δz_{54} , the position trajectory at time t_4 can be determined using Equation (61).

$$z_4 = z_5 - \Delta z_{54} \tag{61}$$

4.4. Find z_3 , t_3 , and t_4

Once the position at time t_4 , z_4 , is known, we can compute the constant C_4 and the position at time t_3 as Equations (62) and (63), respectively.

$$C_4 = z_4 - \ln |n_0 h_1 + n_1 h_2| \tag{62}$$

$$z_3 = \frac{a}{b} \ln |n_0 l_1 + n_1 l_2| + C_4 \tag{63}$$

Based on the information of z_3 and C_3 , time t_3 can be determined using Equation (64).

$$t_3 = \frac{z_3 - C_3}{w_3} \tag{64}$$

Subsequently, time t_4 can be obtained as the sum of time t_3 and the delay caused by the buoyancy engine, as expressed in Equation (65).

$$t_4 = t_3 + \frac{f_{max}}{c_{max}} \tag{65}$$

4.5. Find α and t_5

Using time t_3 , the constant α in the fourth segment can be determined as Equation (66). Subsequently, time t_5 can be calculated based on the boundary constant C_5 , which is derived in Equations (67)–(69).

$$\alpha = t_3 - \frac{f_{max}}{c_{min}} \tag{66}$$

$$C_5 = \frac{-a}{\sqrt{-bf_{min_3}}} \arctan \left(\frac{w_4}{\sqrt{-f_{min}/b}} \right) - t_4 \tag{67}$$

$$C_6 = z_5 \tag{68}$$

$$t_5 = -C_5 \tag{69}$$

The TOT times, namely $t_2, t_3, t_4,$ and $t_5,$ are presented in Equations (49), (64), (65), and (69), respectively. Therefore, if the TOT is chosen as the reference for depth control, the input required will be identical to the design input displayed in Figure 2.

5. Design the Tracking Controller Using the SMC Algorithm

In this section, we introduce the design of a tracking controller for the proposed TOT of the HUG’s depth motion, utilizing the SMC algorithm. The depth trajectory tracking control is depicted in the control system block diagram illustrated in Figure 3. Employing this control strategy ensures the HUG is efficiently guided to the desired depth.

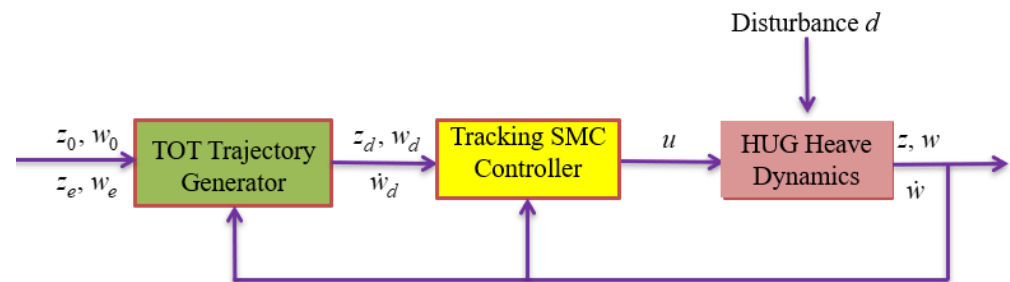


Figure 3. HUG depth control scheme sliding mode control algorithm.

The heave dynamics can be reviewed as follows:

$$\begin{aligned} a\dot{w} + b|w|w &= f + d \\ \dot{z} &= w \end{aligned} \tag{70}$$

where f denotes the control input and d represents the bounded disturbance. It is assumed that the nominal values of the hydrodynamic coefficients for the heave dynamics are known, which allows the controller to focus on dealing with the bounded disturbance d . To achieve this, an SMC with a saturation function was developed for the heave dynamics, as shown below.

The sliding surface s is created as a function of depth error and heave velocity error, represented by Equation (71). The weight λ is a positive value that determines the relative importance of position and velocity error in the control design.

$$s = (w - w_d) + \lambda(z - z_d) \tag{71}$$

The expression for the control input f is obtained as follows.

$$f = \hat{b}w|w| + \hat{a}\dot{w}_d - \lambda\hat{a}(w - w_d) - Ksat\left(\frac{s}{\phi}\right) \tag{72}$$

where \hat{a} and \hat{b} are the assumed nominal values for the system parameters a and b , respectively. The boundary layer for the sliding surface is denoted by ϕ , and K is a positive gain that affects the rate of convergence to the sliding surface.

$$K = \Delta_b w^2 + \Delta_a |\dot{w}_d - \lambda(w - w_d)| + D + \eta a_{max} \tag{73}$$

where the controller assumes that the magnitude of uncertainty in the parameters a and b , represented by Δ_a and Δ_b , respectively, is zero. Additionally, D represents the bound of the external disturbance d , η is a small positive scalar, and a_{max} is the maximum possible value of a .

By utilizing the SMC, the TOT tracking control can be designed to be robust against the effects of external bounded disturbance. The subsequent section aims to demonstrate the effectiveness of combining the TOT and SMC approaches in verifying the tracking performance.

6. Simulation and Discussion

To assess the TOT’s performance and its control input, we conduct a tracking control analysis for the HUG using the SMC algorithm and develop a simulator based on a HUG model. The simulation is implemented using a Matlab-Simulink model comprising three subsystems: one for the designed TOTs and parameters, another for the SMC algorithm, and the third for the heave motion dynamics of the HUG, as illustrated in Figure 4.

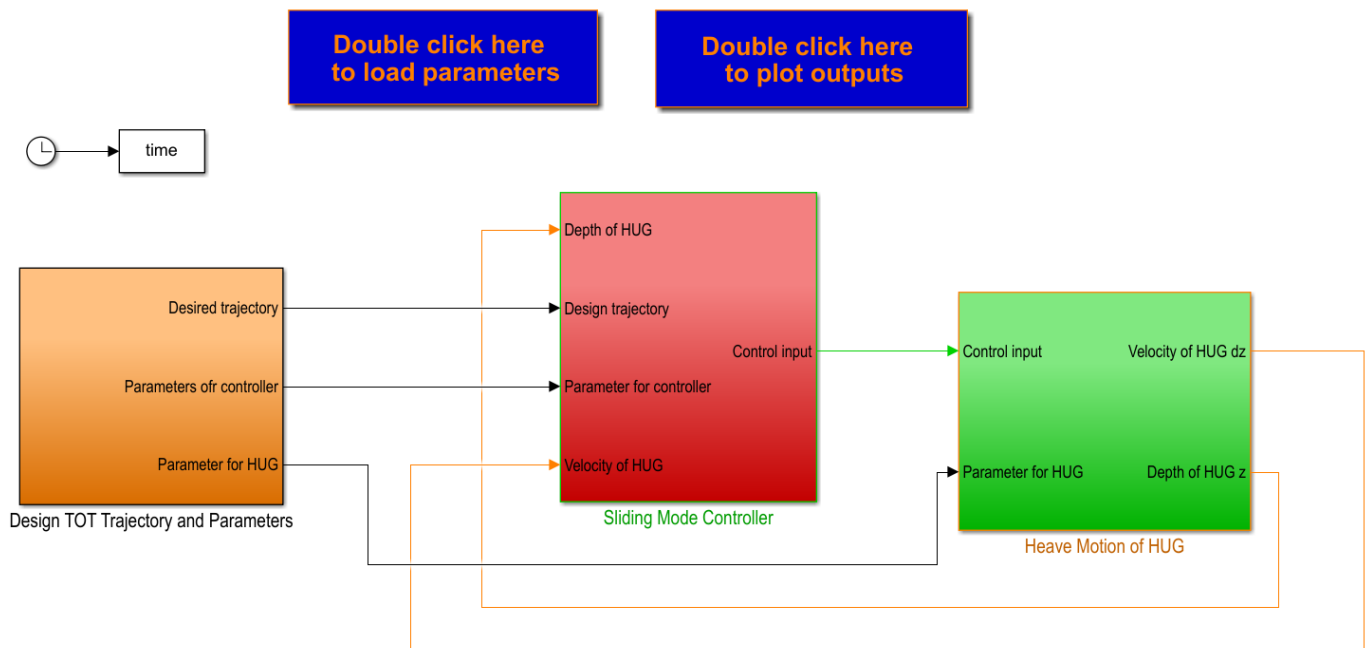


Figure 4. Simulation program.

Table 2 presents the simulation parameters. Simulating the vehicle’s depth control with the proposed TOT and SMC strategy requires utilizing hydrodynamic coefficients and vehicle variables from Vu et al. [29], typically estimated through the CFD method. The values of a , b , f_{max} (net buoyancy force), and f_{min} (including the thruster force and pitch angle) were set to 50.5 kg, 10 kg, 3.43 N, and -10 N, respectively. Additionally, the rate of buoyancy force, an essential parameter of the buoyancy engine, was assumed to be $c_{max} = -c_{min} = \frac{f_{max}}{20}$ N/s, and it takes 20 s to reach the maximum force from zero. To further observe the simulation’s performance, we added a disturbance to the dynamics as $d = 0.2 \sin(2t/\pi)$. This disturbance enabled us to test the TOT control input’s ability to oscillate around the predefined input with the same disturbance magnitude. The SMC, which uses a saturation function, was employed in this depth control simulation.

Table 2. Parameters for simulation.

D (N)	η (m·s ⁻²)	λ (s ⁻¹)	ϕ (m·s ⁻¹)	$Z_{ w w}$ (kgm ²)	$Z_{\dot{w}}$ (kgm ²)	m (kg)	a (kg)	b (kg)	f_{max} (N)	f_{min} (N)
2	0.01	2	0.1	0.0356	-0.0119	50.48	50.5	10	3.43	-10

6.1. Simulation 1: Tracking Control of TOT Using SMC Controller without Disturbance

The desired depth for the simulation was set to 40 m, with $z_0 = 0$ as the water surface and $z_5 = 40$ m as the target depth. To determine the TOT profile, the times t_2 , t_3 , t_4 , and t_5 were obtained using Equations (49), (64), (65), and (69), respectively, resulting in $t_2 = 63.5238$, $t_3 = 66.1899$, $t_4 = 86.1899$, and $t_5 = 87.7597$. In practical scenarios, the depth z_3 at which the buoyancy force must be reversed is crucial to approach the desired depth z_5 in a neutral buoyancy condition. By using Equation (63), depth z_3 was computed as 30.1475 m for this simulation. Hence, by reversing the buoyancy force at $z_3 = 30.1475$ m, the HUG vehicle could achieve the target depth $z_5 = 40$ m in the neutral buoyancy condition.

According to the results depicted in Figure 5, the TOT was accurately tracked by the actual position, velocity, and acceleration. The heave velocity, as illustrated in Figure 5, achieved its maximum value of 0.587 m/s at t_2 . Meanwhile, the heave acceleration initially increased from zero to 0.031 m/s² and then decreased to zero at t_2 . From t_2 to t_4 , the net buoyancy force declined to zero to achieve neutral buoyancy, and the thruster was utilized from t_4 to t_5 . During this period, the buoyancy force decreased from 3.43 N to 0 N in 20 s, resulting in a reduction in heave velocity and heave acceleration to 0.32 m/s and -0.22 m/s², respectively. The thruster was responsible for reducing the velocity and acceleration to zero at t_5 , as shown in Figure 5. After a brief period of operation, the control input of the thruster was set to zero and remained so. As a result, the vehicle's depth was maintained at 40 m using a 3.43 N buoyancy force and -10 N thrust, with a minimum time of 87.8 s. This simulation can be utilized by designers to verify if their buoyancy engine and thruster force capacity designs meet specific requirements for settling time.

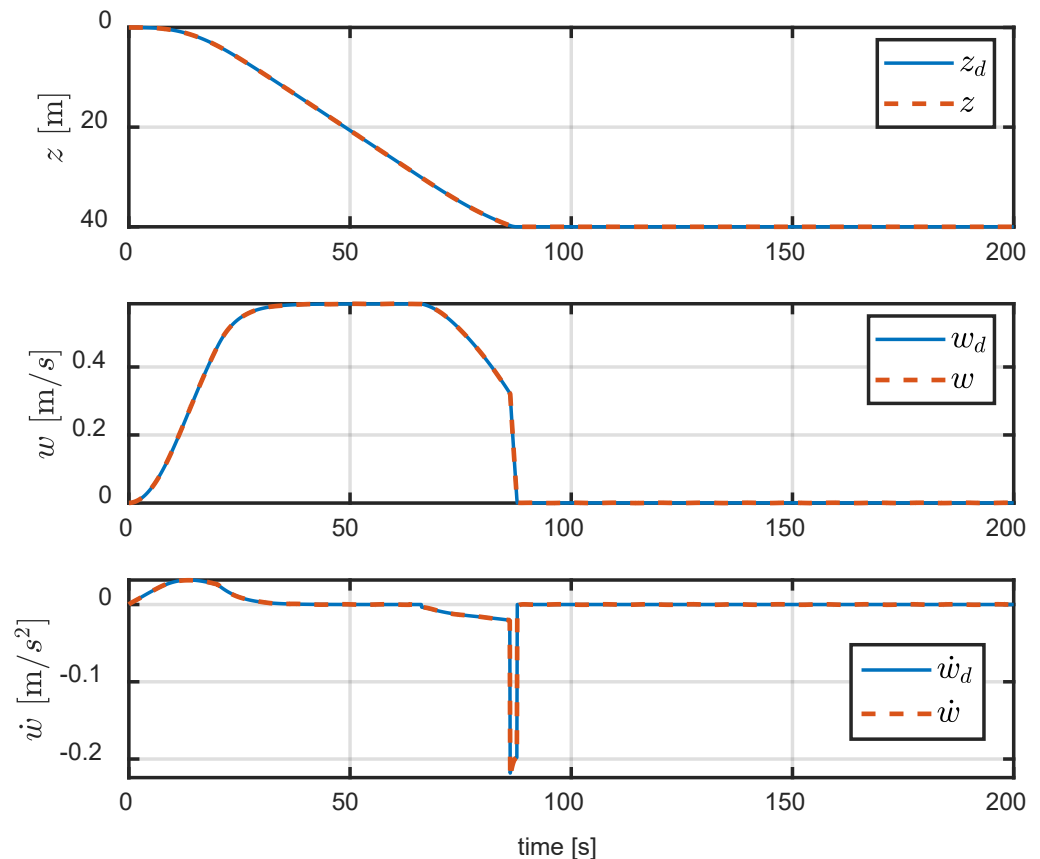


Figure 5. Tracking control performance of TOT using SMC controller without disturbance.

Between time points t_4 and t_5 , the sudden shift in acceleration and velocity trajectories led to a notable spike in the tracking error. Specifically, the position error and velocity error

reached levels of 5×10^{-4} m and 2×10^{-3} m/s, respectively. However, toward the end of the TOT period, all tracking errors gradually subsided and eventually reached zero, as depicted in Figure 6.

As illustrated in Figure 7, the implemented control input closely resembled the pre-planned input. Assuming that the heave dynamics parameters of the actual system match those used in the experiment, utilizing the TOT for control input would push the buoyancy engines and thrusters to their operational limits. By utilizing the full force of these components, it was possible to achieve the shortest possible arrival time for depth control.

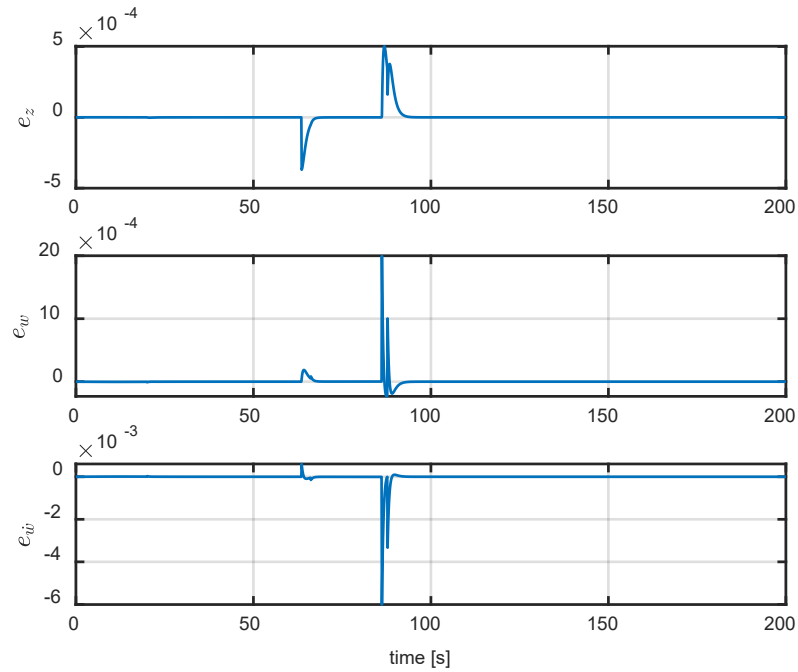


Figure 6. Tracking error of TOT using SMC controller without disturbance.

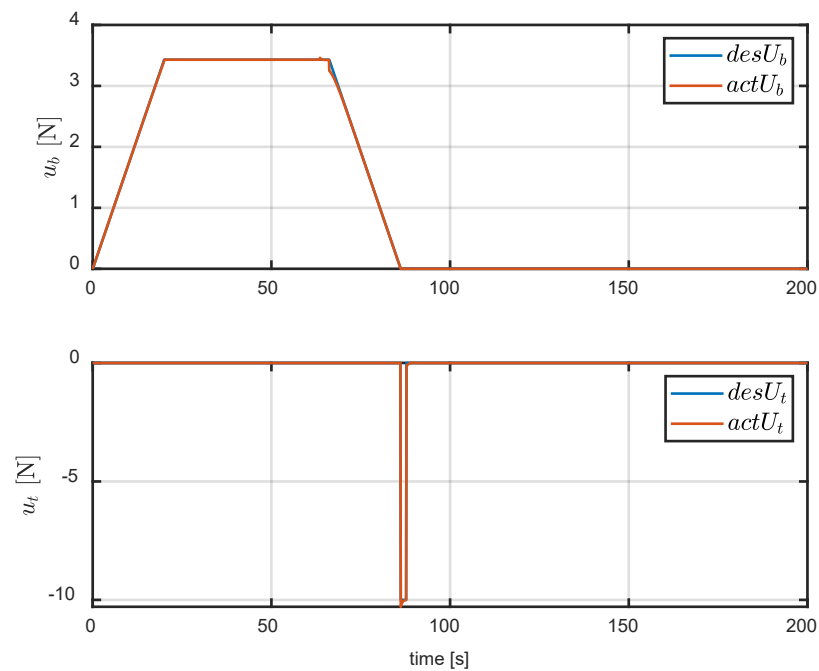


Figure 7. Control input of buoyancy engine and thruster for tracking the TOT without disturbance.

6.2. Simulation 2: Tracking Control of TOT Using SMC Controller under External Disturbance

To evaluate the system’s resilience to external disturbances, we introduced a sinusoidal disturbance ($d = 0.2 \sin(2t/\pi)$) into the heave dynamics via Equation (2). Despite the presence of the disturbance, the TOT tracking performance remained satisfactory, as depicted in Figure 8. However, due to the chattering elimination using the saturation function in SMC, the tracking error deteriorated slightly, as shown in Figure 9. Even so, the position error remained within 0.002 m, while the velocity error and acceleration error were both controlled below 0.002 m/s and 0.006 m/s², respectively.

Figure 10 illustrates the most crucial result of the simulation, where the control input oscillated around the pre-defined input for the TOT due to the disturbance. Moreover, the magnitude of the actual input deviation was equivalent to that of the disturbance. Specifically, the buoyancy force in this simulation fluctuated between 3.22 N and 3.64 N, while the desired input was 3.43 N, as depicted in Figure 10. However, the average value of the actual buoyancy force was estimated to be 3.43 N, which corresponded to the pre-defined input, with a deviation of 0.2 N, equivalent to the magnitude of the disturbance $d = 0.2 \sin(2t/\pi)$. Figure 10 shows the same phenomenon for the thrusting force after completing the TOT. These results suggest that the magnitude of the disturbance must be factored into the buoyancy engine’s design capacity to ensure proper functioning.

The proposed TOT-based depth control algorithm demonstrated robustness against external bounded disturbances, as shown in simulations. This was achieved through the implementation of a robust SMC strategy, incorporating a saturation function to keep the tracking error minimal under such conditions. The control effort closely followed the desired input, and its deviation was equivalent to the disturbance bound. Overall, the TOT-based approach offers a promising solution for robust depth control in the presence of disturbances.

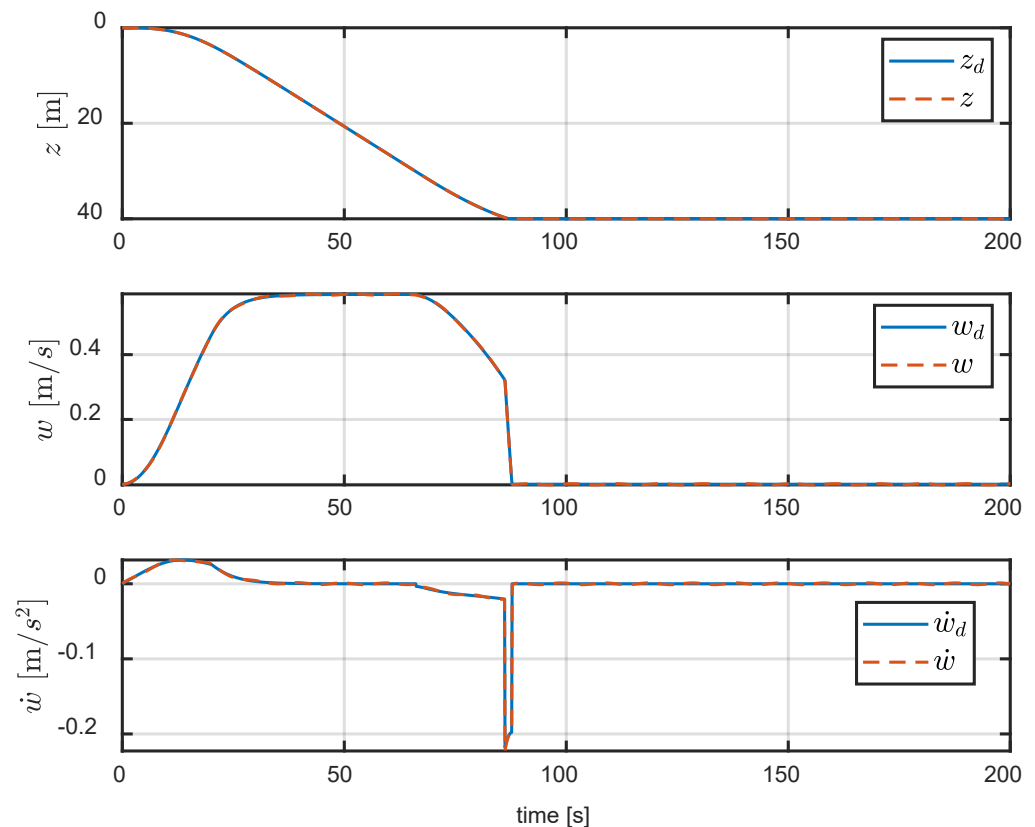


Figure 8. Tracking control performance of TOT using SMC controller with disturbance.

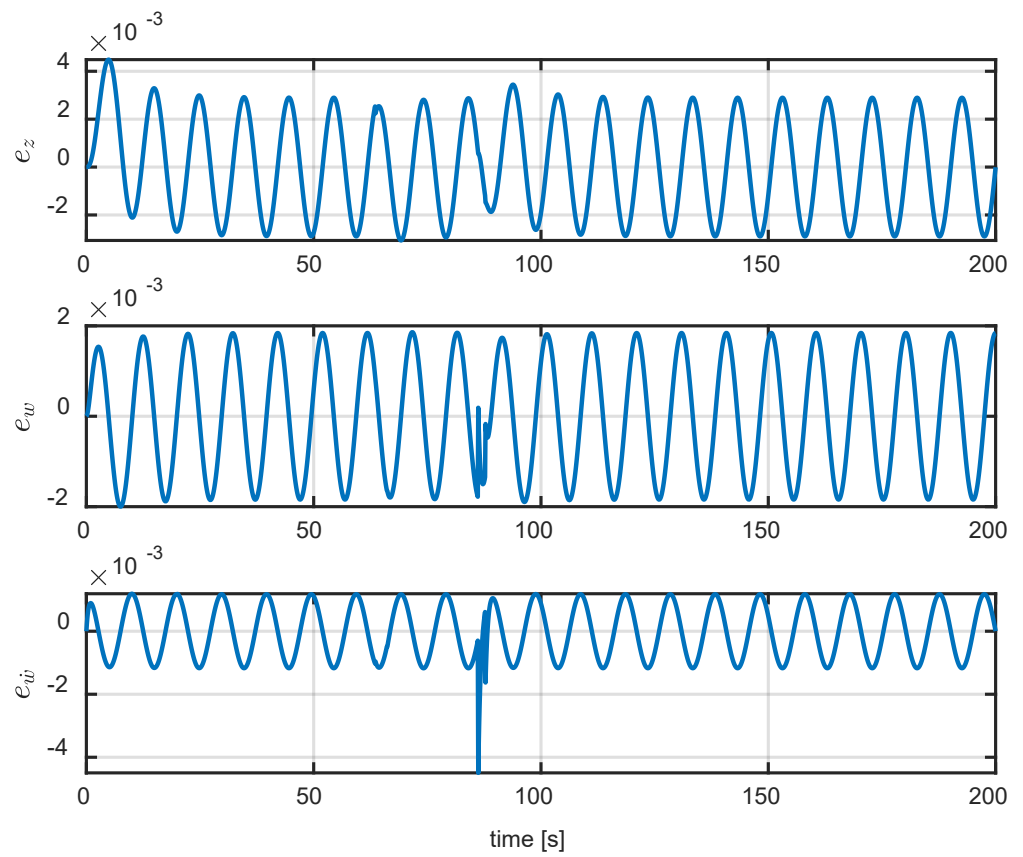


Figure 9. Tracking error of TOT using SMC controller with disturbance.

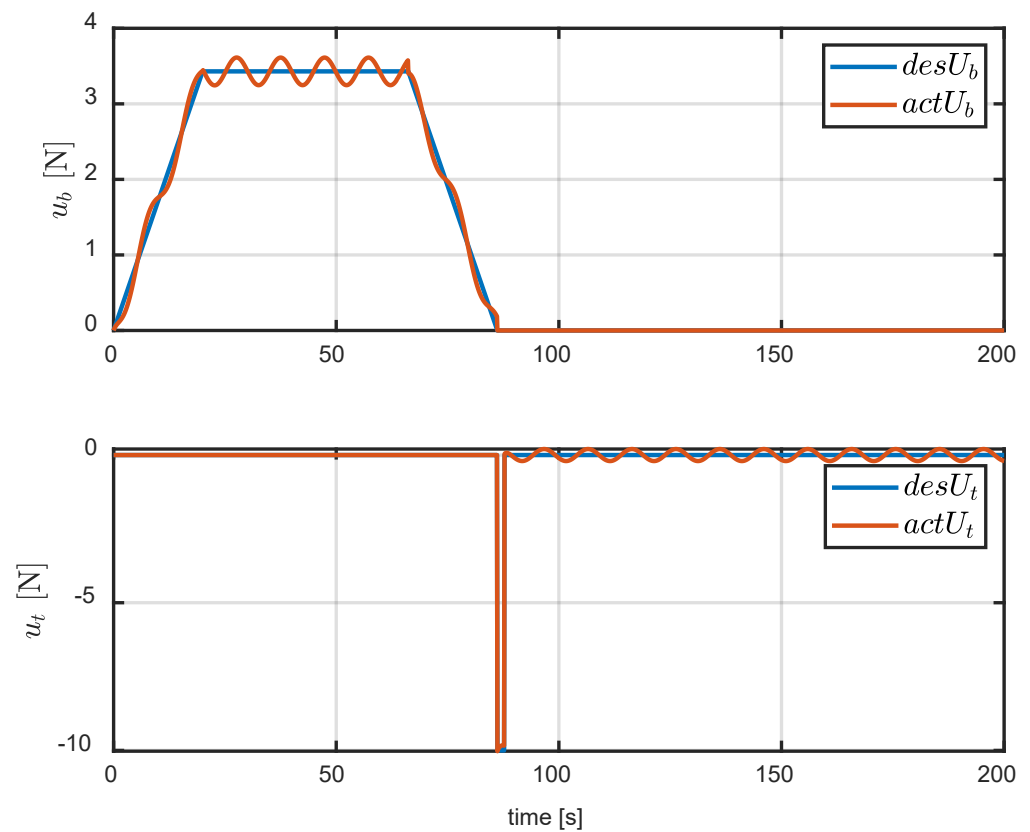


Figure 10. Control input of buoyancy engine and thruster for tracking the TOT with disturbance.

7. Conclusions

The study developed an analytical solution for the TOT in heave dynamics by utilizing a hybrid actuation scheme that incorporated individual buoyancy and thruster forces. It was assumed that the nominal value of the heave dynamics parameters could be estimated; therefore, the analytical solution of heave dynamics could be formulated using the thrusting saturation and constant buoyancy force rate. Then, the shortest trajectory for depth control of a HUG could be established while considering the actuator saturation. The results of the closed-form heave dynamics solution for the buoyancy engine not only shows the TOT for depth control but also provides a formula to compute the depth for reversing the buoyancy force in practical applications. Once the nominal value of the vehicle mass, added mass, and damping coefficients are defined, the proposed TOT helps the HUG reach the desired depth within the shortest arrival time.

The proposed TOT-based robust depth control algorithm was validated in simulations and demonstrated excellent tracking performance even in the presence of bounded disturbances. According to the simulation results, buoyancy and thruster force were used at the maximum and minimum values; therefore, the consuming time in the depth control was the fastest at around 88 s from 0 m to 40 m depth under the assumption that the system parameters and actuator saturations are defined.

The focus of this study was to design the TOT for the HUG system using the buoyancy engine and thruster. Parameter uncertainties were not taken into account in this analysis. However, if the estimation errors of uncertain system parameters are defined as bounded disturbances, the TOT's application can be extended to uncertain HUG systems. This aspect will be the focus of our future work. Also, to further validate the proposed TOT and robust control algorithm, some experiments will be conducted on a physical HUG system.

Author Contributions: Conceptualization, M.T.V. and H.-S.C.; methodology, V.P.N.; software, D.-W.J.; validation, M.T.V., J.H., N.X.-M., V.P.N. and S.H.K.; formal analysis, M.T.V.; investigation, H.-S.C. and M.T.V.; resources, S.H.K. and M.T.V.; data curation, J.H. and N.X.-M.; writing—original draft preparation, S.H.K. and M.T.V.; writing—review and editing, M.T.V.; supervision, H.-S.C. and S.H.K.; project administration, H.-S.C.; funding acquisition, H.-S.C. All authors have read and agreed to the published version of the manuscript.

Funding: This research received no external funding.

Institutional Review Board Statement: Not applicable.

Informed Consent Statement: Not applicable.

Data Availability Statement: Data are contained within the article.

Acknowledgments: This research was supported by the Unmanned Vehicles Advanced Core Technology Research and Development Program through the Unmanned Vehicle Advanced Research Center (UVARC), funded by the Ministry of Science, ICT and Future Planning, the Republic of Korea (No. 2016M1B3A1A02937626). And this research is a part of the project National Research Foundation of Korea (NRF-2016R1A2B4011875).

Conflicts of Interest: The authors declare no conflict of interest.

References

1. Cui, R.; Zhang, X.; Cui, D. Adaptive sliding-mode attitude control for autonomous underwater vehicles with input nonlinearities. *Ocean Eng.* **2016**, *123*, 45–54. [[CrossRef](#)]
2. Vasilijevic, A.; Bremnes, J.E.; Ludvigsen, M. Remote Operation of Marine Robotic Systems and Next-Generation Multi-Purpose Control Rooms. *J. Mar. Sci. Eng.* **2023**, *11*, 1942. [[CrossRef](#)]
3. Lu, C.; Yang, J.; Leira, B.J.; Chen, Q.; Wang, S. Three-Dimensional Path Planning of Deep-Sea Mining Vehicle Based on Improved Particle Swarm Optimization. *J. Mar. Sci. Eng.* **2023**, *11*, 1797. [[CrossRef](#)]
4. Von Benzon, M.; Sørensen, F.F.; Uth, E.; Jouffroy, J.; Liniger, J.; Pedersen, S. An Open-Source Benchmark Simulator: Control of a BlueROV2 Underwater Robot. *J. Mar. Sci. Eng.* **2022**, *10*, 1898. [[CrossRef](#)]

5. Vu, M.T.; Thanh, H.L.N.N.; Huynh, T.T.; Do, Q.T.; Do, T.D.; Hoang, Q.D.; Le, T.H. Station-Keeping Control of a Hovering Over-Actuated Autonomous Underwater Vehicle Under Ocean Current Effects and Model Uncertainties in Horizontal Plane. *IEEE Access* **2021**, *9*, 6855–6867. [[CrossRef](#)]
6. Tang, S.; Xue, N.; Lui, K.; Wang, D.; Ye, J.; Fan, T. Motion control for an open-frame work-class ROV in current using an adaptive super-twisting disturbance observer. *Ocean Eng.* **2023**, *280*, 114723. [[CrossRef](#)]
7. Vu, M.T.; Choi, H.S.; Thieu, Q.M.N.; Nguyen, N.D.; Lee, S.D.; Le, T.H.; Sur, J. Docking assessment algorithm for autonomous underwater vehicles. *Appl. Ocean Res.* **2020**, *100*, 102180. [[CrossRef](#)]
8. Lv, T.; Wang, Y.; Liu, X.; Zhang, M. Command-Filter-Based Region-Tracking Control for Autonomous Underwater Vehicles with Measurement Noise. *J. Mar. Sci. Eng.* **2023**, *11*, 2119. [[CrossRef](#)]
9. Zhang, J.; Ning, X.; Ma, S. An improved particle swarm optimization based on age factor for multi-AUV cooperative planning. *Ocean Eng.* **2023**, *287*, 115753. [[CrossRef](#)]
10. Deutsch, C.; Kutteneuler, J.; Melin, T. Glider performance analysis and intermediate-fidelity modelling of underwater vehicles. *Ocean Eng.* **2020**, *210*, 107567. [[CrossRef](#)]
11. Du, X.; Liu, X.; Song, Y. Analysis of the Steady-Stream Active Flow Control for the Blended-Winged-Body Underwater Glider. *J. Mar. Sci. Eng.* **2023**, *11*, 1344. [[CrossRef](#)]
12. Wu, Q.; Wu, H.; Jiang, Z.; Tan, L.; Yang, Y.; Yan, S. Multi-objective optimization and driving mechanism design for controllable wings of underwater gliders. *Ocean Eng.* **2023**, *286*, 115534. [[CrossRef](#)]
13. Shen, X.R.; Wang, Y.H.; Yang, S.Q.; Liang, Y.; Li, H. Development of underwater gliders: An overview and prospect. *J. Unmanned Undersea Syst.* **2018**, *26*, 89–106.
14. Yang, M.; Wang, Y.; Chen, Y.; Wang, C.; Liang, Y.; Yang, S. Data-driven optimization design of a novel pressure hull for AUV. *Ocean Eng.* **2022**, *257*, 111562. [[CrossRef](#)]
15. Yang, Y.; Liu, Y.; Wang, Y.; Zhang, H.; Zhang, L. Dynamic modeling and motion control strategy for deep-sea hybrid-driven underwater gliders considering hull deformation and seawater density variation. *Ocean Eng.* **2017**, *143*, 66–78. [[CrossRef](#)]
16. Webb, D.C.; Simonetti, P.J.; Jones, C.P. SLOCUM: An underwater glider propelled by environment energy. *IEEE J. Ocean. Eng.* **2001**, *26*, 447–452. [[CrossRef](#)]
17. Wang, Y.; Bulger, C.; Thanyamanta, W.; Bose, N. A Backseat Control Architecture for a Slocum Glider. *J. Mar. Sci. Eng.* **2021**, *9*, 532. [[CrossRef](#)]
18. Sherman, J.; Davis, R.E.; Owens, W.B.; Valdes, J. The autonomous underwater glider “Spray”. *IEEE J. Ocean. Eng.* **2001**, *26*, 437–446. [[CrossRef](#)]
19. Eriksen, C.C.; Osse, T.J.; Light, R.D.; Wen, T.; Lehman, T.W.; Sabin, P.L.; Ballard, J.W.; Chiodi, A.M. Sea glider: A long range autonomous underwater vehicle for oceanographic research. *IEEE J. Ocean. Eng.* **2001**, *26*, 424–436. [[CrossRef](#)]
20. Anderlini, E.; Harris, C.; Phillips, A.B.; Lopez, A.L.; Woo, M.; Thomas, G. Towards autonomy: A recommender system for the determination of trim and flight parameters for Seagliders. *Ocean Eng.* **2019**, *189*, 106338. [[CrossRef](#)]
21. Osse, T.J.; Eriksen, C.C. The deep glider: A full ocean depth glider for oceanographic research. In Proceedings of the Oceans’07, Vancouver, BC, Canada, 29 September–4 October 2007; pp. 1–12.
22. Wang, P.; Wang, X.; Wang, Y.; Niu, W.; Yang, S.; Sun, C.; Luo, C. Dynamics Modeling and Analysis of an Underwater Glider with Dual-Eccentric Attitude Regulating Mechanism Using Dual Quaternions. *J. Mar. Sci. Eng.* **2023**, *11*, 5. [[CrossRef](#)]
23. Jenkins, S.A.; Humphreys, D.E.; Sherman, J.; Osse, J.; Jones, C.; Leonard, N.; Graver, J.; Bachmayer, R.; Clem, T.; Carroll, P.; et al. *Underwater Glider System Study (Technical Report 53)*; Scripps Institution of Oceanography: San Diego, CA, USA, 2003.
24. Tian, X.; Zhang, L.; Zhang, H. Research on Sailing Efficiency of Hybrid-Driven Underwater Glider at Zero Angle of Attack. *J. Mar. Sci. Eng.* **2022**, *10*, 21. [[CrossRef](#)]
25. Wu, X.; Yu, P.; Zhang, C.; Wang, Q.; Zhu, Z.; Wang, T. Shape optimization of underwater glider for maximum gliding range with uncertainty factors considered. *Ocean Eng.* **2023**, *287*, 115869. [[CrossRef](#)]
26. Chyba, M.; Leonard, N.E.; Sontag, E.D. Time-Optimal Control for Underwater Vehicles. *IFAC Proc. Vol.* **2000**, *33*, 117–122. [[CrossRef](#)]
27. Chyba, M.; Haberkorn, T.; Smith, R.N.; Choi, S.K. Design and implementation of time efficient trajectories for autonomous underwater vehicles. *Ocean Eng.* **2008**, *35*, 63–76. [[CrossRef](#)]
28. Rhoads, B.; Mezić, I.; Poje, A.C. Minimum time heading control of underpowered vehicles in time-varying ocean currents. *Ocean Eng.* **2013**, *66*, 12–31. [[CrossRef](#)]
29. Vu, M.T.; Choi, H.S.; Kang, J.I.; Ji, D.H.; Joong, H. Energy efficient trajectory design for the underwater vehicle with bounded inputs using the global optimal sliding mode control. *J. Mar. Sci. Technol.* **2017**, *25*, 705–714.
30. Nguyen, N.D.; Vu, M.T.; Nguyen, P.; Huang, J.; Jung, D.W.; Cho, H.; Phan, H.N.A.; Choi, H.-S. Time-Optimal Trajectory Design for Heading Motion of the Underwater Vehicle. *J. Mar. Sci. Eng.* **2023**, *11*, 1099. [[CrossRef](#)]
31. Koubaa, Y.; Boukattaya, M.; Damak, T. Adaptive sliding mode control for nonholonomic mobile robot with uncertain kinematics and dynamics. *Appl. Artif. Intell.* **2018**, *32*, 924–938. [[CrossRef](#)]
32. Vu, M.T.; Van, M.; Bui, D.H.P.; Do, Q.T.; Huynh, T.T.; Lee, S.D.; Choi, H.S. Study on Dynamic Behavior of Unmanned Surface Vehicle-Linked- Unmanned Underwater Vehicle System for Underwater Exploration. *Sensors* **2020**, *20*, 1329. [[CrossRef](#)]

33. Vu, M.T.; Le, T.H.; Thanh, H.L.N.N.; Huynh, T.T.; Van, M.; Hoang, Q.D.; Do, Q.T. Robust Position Control of an Over-actuated Underwater Vehicle under Model Uncertainties and Ocean Current Effects Using Dynamic Sliding Mode Surface and Optimal Allocation Control. *Sensors* **2021**, *21*, 747. [[CrossRef](#)] [[PubMed](#)]
34. Zhang, X.; Zhou, H.; Fu, J.; Wen, H.; Yao, B.; Lian, L. Adaptive integral terminal sliding mode based trajectory tracking control of underwater glider. *Ocean Eng.* **2023**, *269*, 113436. [[CrossRef](#)]
35. Zhang, W.; Wu, W.; Li, Z.; Du, X.; Yan, Z. Three-Dimensional Trajectory Tracking of AUV Based on Nonsingular Terminal Sliding Mode and Active Disturbance Rejection Decoupling Control. *J. Mar. Sci. Eng.* **2023**, *11*, 959. [[CrossRef](#)]
36. Sahu, B.K.; Subudhi, B. Adaptive tracking control of an autonomous underwater vehicle. *Int. J. Autom. Comput.* **2015**, *11*, 299–307. [[CrossRef](#)]
37. Li, J.H.; Lee, P.M. Design of an adaptive nonlinear controller for depth control of an autonomous underwater vehicle. *Ocean Eng.* **2005**, *32*, 2165–2181. [[CrossRef](#)]
38. Park, B.S.; Kwon, J.-W.; Kim, H. Neural network-based output feedback control for reference tracking of underactuated surface vessels. *Automatica* **2017**, *77*, 353–359. [[CrossRef](#)]
39. Chiman, K.; Lewis, F.L. Robust backstepping control of nonlinear systems using neural networks. *IEEE Trans. Syst. Man. Cybernetics* **2000**, *30*, 753–766.
40. Thanh, H.L.N.N.; Vu, M.T.; Mung, N.X.; Nguyen, N.P.; Phuong, N.T. Perturbation Observer-Based Robust Control Using a Multiple Sliding Surfaces for Nonlinear Systems with Influences of Matched and Unmatched Uncertainties. *Mathematics* **2020**, *8*, 1371. [[CrossRef](#)]
41. Li, J.; Du, J.; Chang, W.-J. Robust time-varying formation control for underactuated autonomous underwater vehicles with disturbances under input saturation. *Ocean Eng.* **2019**, *179*, 180–188. [[CrossRef](#)]
42. Liang, X.; Qu, X.; Wang, N.; Zhang, R.; Li, Y. Three-dimensional trajectory tracking of an underactuated AUV based on fuzzy dynamic surface control. *IET. Intell. Transp. Syst.* **2019**, *14*, 364–370. [[CrossRef](#)]
43. Zhong, Y.; Yang, Y.; He, K.; Chen, C. Fast terminal sliding-mode control based on unknown input observer for the tracking control of underwater vehicles. *Ocean Eng.* **2022**, *264*, 112480. [[CrossRef](#)]
44. Rojsiraphisal, T.; Mobayen, S.; Asad, J.H.; Vu, M.T.; Chang, A.; Puangmalai, J. Fast Terminal Sliding Control of Underactuated Robotic Systems Based on Disturbance Observer with Experimental Validation. *Mathematics* **2021**, *9*, 1935. [[CrossRef](#)]
45. Claus, B.; Bachmayer, R.; Cooney, L. Analysis and development of a buoyancy-pitch based depth control algorithm for a hybrid underwater glider. In Proceedings of the 2012 IEEE/OES Autonomous Underwater Vehicles (AUV), Southampton, UK, 24–27 September 2012; pp. 1–6.
46. Fossen, T.I. *Guidance and Control of Ocean Vehicles*; John Wiley & Sons: New York, NY, USA, 1994.
47. Fossen, T.I. *Handbook of Marine Craft Hydrodynamics and Motion Control*; John Wiley & Sons: Hoboken, NJ, USA, 2011.

Disclaimer/Publisher’s Note: The statements, opinions and data contained in all publications are solely those of the individual author(s) and contributor(s) and not of MDPI and/or the editor(s). MDPI and/or the editor(s) disclaim responsibility for any injury to people or property resulting from any ideas, methods, instructions or products referred to in the content.